Article

Study on Surface Roughness of Sidewall When Micro-Milling LF21 Waveguide Slits

Xiaohong Lu [ID]**, Pengrong Hou *, Yihan Luan, Xudong Sun, Jinhui Qiao and Yu Zhou**

School of Mechanical Engineering, Dalian University of Technology, Dalian 116024, China; lxhdlut@dlut.edu.cn (X.L.); lyhdlut@mail.dlut.edu.cn (Y.L.); sxd@mail.dlut.edu.cn (X.S.); qiaojinhui1997@mail.dlut.edu.cn (J.Q.); zhouyu_@mail.dlut.edu.cn (Y.Z.)
* Correspondence: hprdlut@mail.dlut.edu.cn

Abstract: The surface quality of the sidewall in waveguide antennae is important, especially surface roughness, which directly affects the electrical performance of the slotted waveguide antenna. Micro-milling is a potentially effective processing technique for the antenna. However, surface roughness has been difficult to guarantee within a reasonable accuracy range. In this study, orthogonal experiments of micro-milling LF21 waveguide slits were conducted. The results of the range analysis mainly sorted the factors that affected the surface roughness and also helped to determine how surface roughness could be kept at a minimum. The surface roughness was predicted by using the group method of data handling (GMDH). The importance of the applied GMDH was that it continuously adjusted the network structure according to the potential relationship between cutting parameters and the corresponding surface roughness, which helped determine the model most optimally fitted to the experimental data. This research can be used as a reference for selecting cutting parameters in micro-milling LF21.

Keywords: LF21; micro-milling; fine seam; surface roughness of sidewall

1. Introduction

LF21 has high electrical conductivity, plasticity, etch-resistant ability and solderability, which explains why it is widely used in slotted waveguide antennae [1]. However, its low strength and hardness mean that it has poor cutting properties and is prone to plastic flow under cutting forces, resulting in machinery defects such as material extrusion and build-up [2]. The surface roughness of the sidewall in waveguide slits has a significant influence on the electrical performance of the waveguide antenna. To explain, Ra is required to be less than 0.8 μm [3]. Generally, micro-milling is used to manufacture high-precision parts with dimensions between 100 μm and 10 mm [4]. In the previous study, we achieved 0.2 μm Ra for the sidewall when micro-milling Inconel 718 [5], which strongly confirmed that micro-milling was a potential effective processing technology for the manufacturing of LF21 waveguide slits. However, the finished surface roughness is difficult to control due to rapid tool wear and the complex, dynamic characteristics of micro-milling. More importantly, elastic recovery, cutting-edge radius effects, tool runout, switching between plough and shear states with minimum cutting thickness, etc., can lead to the output of complex cutting forces and cutting heat, which ultimately have a direct impact on the surface roughness of sidewalls [6–8]. This necessitates further analysis of the potential relationship between surface roughness and cutting parameters in the micro-milling of LF21 waveguide slits, although this would be challenging in light of the complicated physics and mechanics involved in the milling process and the material response.

One way to reduce the attention to physics and mechanics in machining is to take an end-to-end approach, i.e., to investigate statistical learning models on cutting parameters and surface roughness. V.S. Sooraj et al. [9] found that the spindle speed and feed per tooth

significantly affected surface roughness when micro-end-milling brass; J.H. Ko et al. [10] also found that the effects of spindle speed and feed per tooth on the surface roughness of the processed sidewall were more obvious than the axial depth of cut during the micro-end-milling of SUS 304 and Al 6061. Many scholars have developed mathematical–statistical models on micro-milling surface roughness. Lu et al. [11] developed a surface roughness prediction model on the micro-milling of Inconel 718 using the response surface method in 2018 and indicated that the parameters impacting surface roughness, from high to low, were cutting depth, feed rate and spindle speed. W.T. Shi [12] proposed a prediction model on surface roughness based on the dual response surface method during the micro-milling of hard aluminum alloys. C. Burlacu et al. [13] established a prediction model on surface roughness based on the micro-milling of a C45W steel groove bottom, using the multiple regression method.

Artificial neural networks (ANNs) lie at the frontier of complex, nonlinear science and artificial intelligence science. They establish complex and nonlinear relationships among variable parameters, which are too difficult to achieve by conventional models. C. Bandapalli et al. [14] presented a prediction of surface roughness using back-propagation, feed-forward neural network (BPNN), the Levenberg–Marquardt algorithm (LMA), the group method of data handling (GMDH) and multiple regression analysis (MRA) in the high-speed micro-end-milling of titanium alloy (grade 5). It has been shown that the prediction accuracy of a neural network is higher than the accuracy of the other methods. Furthermore, C. Bandapalli et al. [15] proposed that using the adaptive neuro-fuzzy inference system (ANFIS) methodology to establish a prediction model on surface roughness was reasonable, since it could generate prediction accuracy that reached 99.96% by using the general bell membership function. Yazid Abdulsameea Mohammed Saif [16] used an ANN to establish an optimal model on surface roughness during micro-end-milling. Research has shown that the ANN method is more suitable for the prediction of surface roughness in the micro-milling process.

The GMDH on a polynomial basis is a feed-forward neural network commonly used for data mining, knowledge discovery, the prediction of complex system modeling, optimization and pattern recognition. It has higher stability compared with other ANNs, as it is capable of adaptive synthesis by automatically filtering the model's structure and its variables, for example, avoiding the over-fitting and under-fitting of the model structure, and reducing the influence of subjective factors on the network. Moreover, it can express the functional relationship of input and output as polynomial-based equations. These explicit model equations reveal the correlation and dependence amongst the variables [17]. Therefore, it is appropriate to apply the GMDH to surface-roughness prediction.

In summary, spindle speed and feed per tooth have a significant effect on the surface roughness in micro-milling. As far as we know, previous work has focused only on the surface roughness of sidewalls when micro-milling slots, i.e., only the Ra obtained after single machining is studied when, actually, the study of surface roughness is of critical significance for revealing machining mechanisms. We conducted experiments on the micro-milling of LF21-slotted waveguide antennae and studied the influence principle of cutting parameters (i.e., the spindle speed and the feed per tooth) on surface roughness. Furthermore, we built a surface-roughness prediction model based on the GMDH. In the construction of this model, machining output variables and input variables such as spindle speed and feed per tooth were considered with regard to surface roughness. The quadratic K-g polynomial was also selected, along with the Regularization criterion, i.e., organizing the reference function and the screening during the training process for the GMDH. The results signified that the GMDH model helped to produce surface-roughness predictions with a high level of accuracy.

2. Materials and Methods

2.1. Experimental Procedure

2.1.1. Experimental Device

Experiments were conducted on a self-developed, three-axis and vertical micro-milling machine (Figure 1). The body size of the machine was 194 mm (X) × 194 mm (Y) × 400 mm (Z), and the workspace size was 50 mm (X) × 50 mm (Y) × 102 mm (Z). The spindle speed ranged from 40,000 rpm to 140,000 rpm. The absolute-position accuracy of the feed system was 1 µm, and the repeat-position accuracy was 0.2 µm. The Tungsten–Carbide-coated, flat-end mill made by the Nisshin Scientia company was adopted with a diameter of 300 µm (MSE 230). The material compositions of the LF21 are shown in Table 1. The size of the LF21 workpiece was 15 mm (X) × 40 mm (Y) × 0.5 mm (Z). The surface roughness of the micro-milled surface was measured by a confocal laser microscope, made by the Keyence company (VK-X200). The optical resolution of the instrument was 0.5 nm min. The 3D surface topography and the 2D surface roughness of the LF21 sidewall micro-milling are shown in Figure 2a,b, respectively. The arithmetic means deviation of the contour of the Ra was used to evaluate the surface roughness of the sidewall surface.
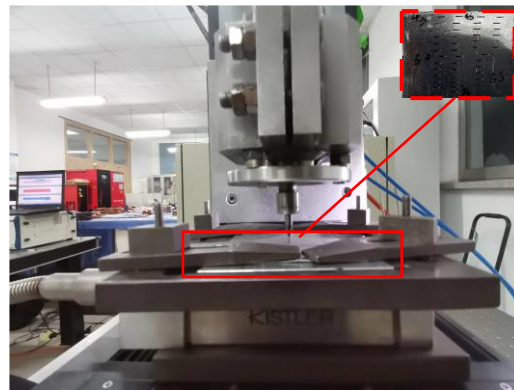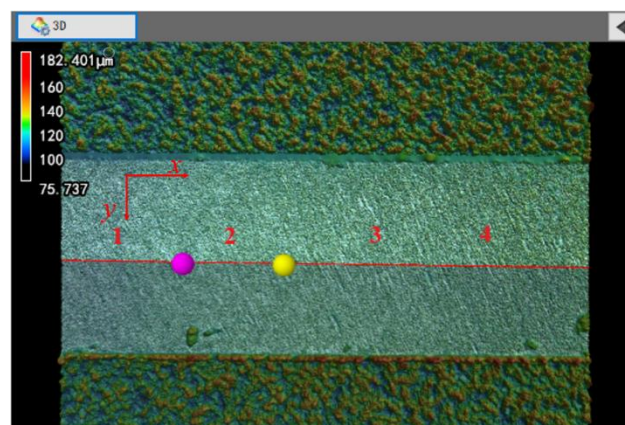

Figure 1. The micro-milling machine tool.

Table 1. Materials composition of LF21.

	Thermal Conductivity $(\mathrm{W}/(\mathrm{m}\cdot\mathrm{°C}))$	Coefficient of Thermal Expansion $(1/\mathrm{°C})$	Modulus of Elasticity (Mpa)	Thermal Capacity $(\mathrm{N}/(\mathrm{mm}^2\cdot\mathrm{°C}))$	Poisson's Ratio	Hardness
LF21	180.2	2.2×10^{-5}	6.86×10^4	2.433	0.25	11

(**a**)

Figure 2. *Cont*.

(**b**)
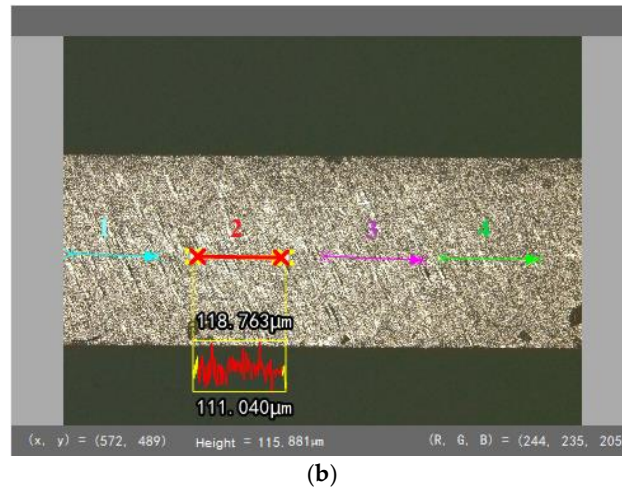
Figure 2. Surface roughness measurement at 65,000 rpm and 0.2 µm/z. (**a**) Three-dimensional topography of sidewall surface. (**b**) Two-dimensional surface.

Where x and y represent the feed and the depth of cut directions. The averages of the surface roughness values, measured at 4 equidistant locations on each slot, were used for the analysis.

2.1.2. Process Setup

The experiments were conducted using the Design of Experiment (DoE) methodology. We conducted an orthogonal trial with a mixed-level design utilising two factors: the spindle speed n and the radial depth of the cut ae. The above experiments were conducted to understand the effect of cutting parameters on surface roughness. Table 2 shows the selection of cutting parameters.

Table 2. Process window.

	Lower Limit		Upper Limit
Spindle speed	40,000 rpm		65,000 rpm
Feed per tooth	0.2 µm/z		0.6 µm/z
Cutting depth in the axial direction		20 µm	
Extended length of the tool		20 mm	

2.2. Artificial Neural Networks

The GMDH was applied for the mathematical modeling of multi-parametric datasets, which is characterized by an inductive procedure of extending and developing the network until the working efficiency of the network reaches the desired point during the learning process [18]. That is, the network structure was not fixed during the training. The structure sample of the GMDH method for the surface-roughness prediction for the micro-milling of brass is shown in Figure 3 [19].
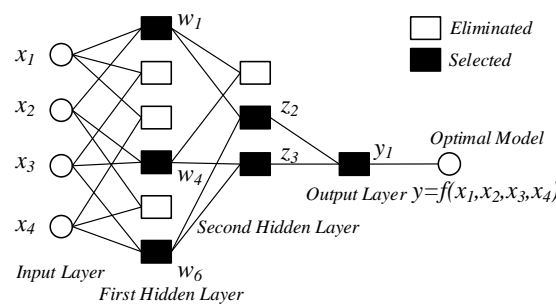
Figure 3. Structure sample of GMDH for surface roughness prediction.

Where x_1, x_2, x_3 and x_4 represent the extended length of the micro-milling tool, spindle speed, feed per tooth and cutting depth in the axial direction. y_1 is an explicit model equation, which represents the surface-roughness prediction model.

Figure 3 depicts an example structure of the GMDH used in the prediction of surface roughness. The network has four inputs and one output above. The input layer of the GMDH network forwards the input signal to the middle layer (that is, the first hidden layer and the second hidden layer). Each neuron in the middle layer corresponds to two neurons in the previous layer. Therefore, there must be only two neurons in the previous layer (the middle layer) of the output layer.

Generally, only select, adaptive and linear elements as neurons of the GMDH network, as shown in Figure 4, are considered. That is, only the functions of the two variables (neurons) in linear, polynomial and quadratic forms are considered. The following Equation (1) represents the quadratic form:

$$Z_{k,l} = F(Z_{k-1,i}, Z_{k-1,j}) = a_0 + a_1 Z_{k-1,i} + a_2 Z_{k-1,j} + a_3 Z_{k-1,i} Z_{k-1,j} + a_4 Z_{k-1,i}^2 + a_5 Z_{k-1,j}^2 \tag{1}$$

where $Z_{k,l}$ represents the lth processing unit of the kth layer and the coefficients of $a_0 - a_5$ can be calculated by minimizing the root mean square error (*RMSE*), given in Equation (2) by multiple regression analysis.

$$RMSE = \sqrt{\frac{\sum\limits_{i=1}^{n}(z_{k,l} - Z_{k,l})^2}{n}} \tag{2}$$

where $Z_{k,l}$ shows actual data. In this study, we developed an explicit equation that predicted surface roughness based on the GMDH method. The flow chart of surface roughness prediction by GMDH methodology is shown in Figure 5. The given steps were followed to create the model equations utilizing the GMDH algorithm.

1. Prepare the dataset. Arrange the dataset part of learning (Part A) $\{x_i, y_i\}$, testing (Part B) $\{x_j, y_j\}$ and predicting (Part C) $\{x_k, y_k\}$, obtained by the micro-milling experiments, where the sample data in Table 1 are dynamically divided into Part A and Part B. Part C comes from the new sample data and not those used to establish the model. Use Part A to generate the model to be selected, Part B to verify and filter the generated model and Part C to verify the surface roughness model. x is a multi-dimensional input variable that consists of the spindle speed and the feed per tooth. y is the output variable, which is the roughness measurement obtained by the test.

2. Preprocess the dataset above, that is, normalize the dataset and remove the static DC component. Generally, for the existing dataset, the following transformation is performed before the training of the neural network:

$$\begin{cases} x_i^* = \frac{x_i - \bar{x}}{\sigma_x} \\ y_i^* = \frac{y_i - \bar{y}}{\sigma_y} \end{cases} \tag{3}$$

where x_i and y_i are the values before preprocessing, $\bar{x}$ and $\bar{y}$ are the average values of x_i and y_i, σ_x and σ_y are standard deviations of x_i and y_i.

3. Select the reference function and external criterion. Establish the general relationship between the dependent variable (output) and the independent variable (input) as a reference function. Select the quadratic K-g polynomial (Equation (1)) as a reference function and the Regularization criterion (Equation (4)) as the basis of screening:

$$\Delta_B = \frac{1}{N_B}\|y_B - X_B \hat{a}_A\|^2 \tag{4}$$

where Δ_B is the criterion value of the equation in Part B, N_B is the number of experiments in Part B, y_B is the measured value obtained by the test, X_B is the cutting parameter corresponding to y_B and $\hat{a}_A$ represents the estimated coefficients in Part A.

4.　Determine the transfer function. Using the reference function, obtain the initial model function of network structures (Equation (5)), fit the equation of output variables for x_i and x_j by RMSE in Part A, estimate the coefficients of $a_0 - a_5$, and then calculate the criterion value of the equation in Part B.

$$
\begin{aligned}
y &= a_0 \\
y &= a_0 + a_1 x_i \\
y &= a_0 + a_1 x_i + a_2 x_j \\
y &= a_0 + a_1 x_i + a_2 x_j + a_3 x_i x_j \\
y &= a_0 + a_1 x_i + a_2 x_j + a_3 x_i x_j + a_4 x_i^2 \\
y &= a_0 + a_1 x_i + a_2 x_j + a_3 x_i x_j + a_4 x_i^2 + a_5 x_j^2
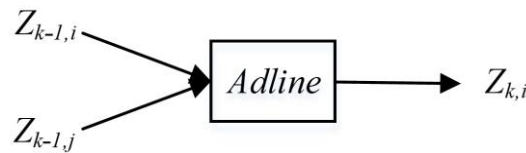\end{aligned}
\tag{5}
$$

Figure 4. Neuron in the GMDH network (except input-layer neurons).

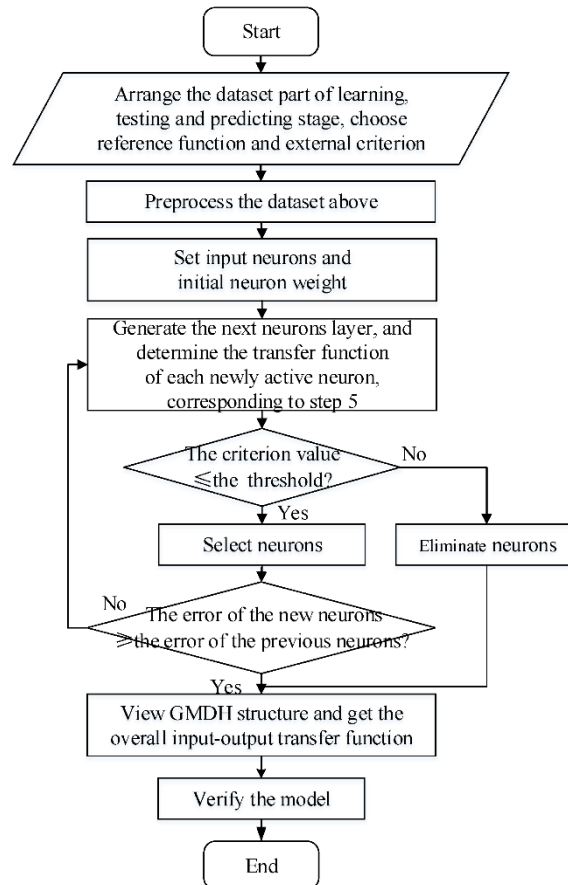**Figure 5.** Flow chart for prediction of surface roughness by GMDH.

When finding out the minimum deviation criterion, use the critical local function, corresponding to the criterion, as the transfer function of the active neuron.

5.　Screen for intramolecular neurons. For m × (m − 1)/2, active neurons generated by m input neurons are in the input layer. Confirm and screen them according to the

criterion value in Part B. Determine the number of selected neurons by ensuring the criterion value is less than a certain threshold. In this study, the threshold is set as root mean square error in Part A and Part B. The selected neurons will continue to participate in the next generation of neurons, while those that are not selected will be eliminated.

6. Obtain the optimal complexity model network structure. Use the neurons selected in each layer, that is, those closest to the output layer as new input neurons. This is similar to step 5 and step 6 and will create a new generation of neurons in pairs. When the error in the new generation of neurons is no less than that of the previous generation, the optimal network structure will be found. Select the neuron with the smallest criterion value in the last layer and deduct its transfer function, step by step, to obtain the explicit model equation for between the output variable and the input variable.

7. Verify the validity of the model. For the evaluation of the accuracy of the established model, use Part C to predict the surface roughness.

3. Results

3.1. Experimental Results

The combination of cutting parameters and the experimental results are presented in Table 3. The surface roughness Ra ranged from 0.842 μm to 1.481 μm. The experimental value of the surface roughness Ra was fitted with the input variable, using the cubic interpolation method (based on MATLAB), and these results are shown in Figure 6.

Table 3. Experimental results of micro-milling LF21.

Group	Spindle Speed (rpm)	Feed per Tooth (μm/z)	Cutting Depth in the Axial Direction (μm)	Extended Length of Tool (mm)	Surface Roughness (μm)
1	40,000	0.2	20	20	1.271
2	40,000	0.4	20	20	1.350
3	40,000	0.6	20	20	1.275
4	45,000	0.2	20	20	1.375
5	45,000	0.4	20	20	1.481
6	45,000	0.6	20	20	1.327
7	50,000	0.2	20	20	0.962
8	50,000	0.4	20	20	1.048
9	50,000	0.6	20	20	0.810
10	55,000	0.2	20	20	1.007
11	55,000	0.4	20	20	0.925
12	55,000	0.6	20	20	0.869
13	60,000	0.2	20	20	1.211
14	60,000	0.4	20	20	1.462
15	60,000	0.6	20	20	1.119
16	65,000	0.2	20	20	1.165
17	65,000	0.4	20	20	1.380
18	65,000	0.6	20	20	0.842

It was observed that when the spindle speed was constant at 50,000 rpm with 0.2 μm/z, 0.4 μm/z and 0.6 μm/z feed per tooth, the surface roughness was almost constant and smaller. Initially, the cutting temperature in the shear zone may have increased significantly along with the increasing spindle speed, which may have resulted in a decrease in the yield strength, chip thickness, and tool-chip contact length of the workpiece material, with a consequent decrease in surface roughness. As the spindle speed increased further, the surface harshness expanded continuously, as can be seen from the increase in the feed rate and the chip cross-section. When the feed per tooth was constant at 0.4 μm/z with 40,000 rpm, 45,000 rpm, 50,000 rpm, 55,000 rpm, 60,000 rpm and 65,000 rpm spindle speeds,

the surface roughness was higher. Theoretically, roughness increases with the increase in feed per tooth. However, in the case of LF21, the sensitivity of the surface roughness to the cutting parameters may have been different at high feed rates. This is because of the problem of chip evacuation, caused by the sticking tendency and thermal softening of LF21. The increase in cutting temperatures with the increase in feeds per tooth may have influenced the surface roughness.
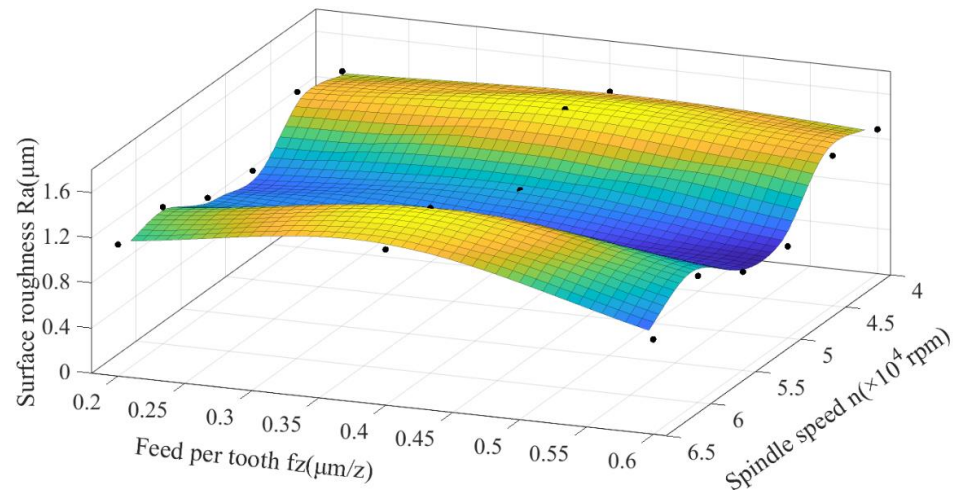
Figure 6. Surface roughness under the cutting parameters of Table 1.

Based on Table 3, the range analyses were performed to obtain the average response from the surface roughness of the micro-milled LF21 sidewall, as shown in Table 4.

Table 4. The average responses of the surface roughness of sidewall.

No	Spindle Speed (rpm)	Feed per Tooth (μm/z)
1	1.2987	1.1652
2	1.3943	1.2743
3	0.9400	1.0403
4	0.9337	
5	1.2640	
6	1.1290	
Range	0.4607	0.2340

The parameters impacting the surface roughness from high to low were spindle speed and feed per tooth, based on the average response table, which was consistent with the research results above [5]. Furthermore, the optimal combination of surface roughness was a spindle speed of 50,000 rpm and a feed per tooth of 0.6 μm/z.

3.2. Additional Value of Process Data

Table 5 shows the predictive values and the measured values. It can be seen from Table 5 that the maximum relative error was 28.78% and the average relative error was 12.41%, having used the GMDH model on surface roughness established in this study. These results indicate that the training for the GMDH method allowed for reasonable accuracy when predicting surface roughness.

Table 5. Predicted and measured surface roughness.

No	Spindle Speed n/(rpm)	Feed per Tooth f_z/(μm/z)	Cutting Depth in the Axial Direction /(μm)	Extended Length of the Tool L/(mm)	Measured Value Ra/μm	Predictive Value Ra/μm	Error
1	37.68	0.1	20	20	1.004	0.982	2.20%
2	42.39	0.3	20	20	1.552	1.263	18.64%
3	47.10	0.5	20	20	0.932	1.200	28.78%
4	51.81	0.1	20	20	0.958	0.982	2.49%
5	56.52	0.3	20	20	1.402	1.263	9.94%
	Mean relative error						12.41%

4. Conclusions

This paper used a GMDH neural network to predict the surface roughness of sidewalls when micro-milling LF21 waveguide slits. The present work included the estimation of the optimal values for the process factors, such as spindle speed and feed per tooth, while the surface roughness was taken as the output. Experiments were conducted to verify the accuracy of the model; the maximum relative error was 21.22% and the average relative error was 13.92%. The obtained results prove the ability of the GMDH method for micro-milling modeling. In the final validation of the predictive models, through another machining test, the GMDH model helped us to find that the external criterion and threshold selection had a great influence on model accuracy. This paper's contributions are its influence on breaking conventional thinking by confirming that milling is not the only option and that micro-milling can be considered during the machining of waveguide slits. Within a specific range of cutting parameters, we argue that the spindle speed had a more significant effect on the surface roughness of the sidewall in the slit than the feed per tooth. We have confirmed that the GMDH can be used to predict the surface roughness of the sidewall when micro-milling a waveguide slit. It is encouraged to further refine the range of cutting parameters and to seek the optimal combination to meet the requirements of the sidewall when micro-milling waveguide slits, to ensure processing efficiency.

The shortcomings of this paper are that the effects of the extended length of the tool and the single cutting depth in the axial direction for the surface roughness of sidewall are not considered.

Author Contributions: Conceptualization, X.L. and P.H.; methodology, P.H.; software, P.H.; validation, Y.L.; formal analysis, Y.L.; investigation, X.S.; data curation, Y.L., J.Q. and Y.Z.; writing—original draft preparation, P.H.; writing—review and editing, X.L.; project administration, X.L.; funding acquisition, X.L. All authors have read and agreed to the published version of the manuscript.

Institutional Review Board Statement: Not applicable.

Informed Consent Statement: Not applicable.

Data Availability Statement: Not applicable.

Conflicts of Interest: The authors declare no conflict of interest.

References

1. Wang, Z.H.; Yuan, J.T.; Hu, X.Q.; Huang, J. Experimental study on milling forces in high-speed end milling of lf21 aluminum alloy. *Chin. Mech. Eng.* **2009**, *20*, 1660–1664.
2. Rahman, M.A.; Rahman, M.; Kumar, A.S. Material perspective on the evolution of micro-and nano-scale cutting of metal alloys. *J. Manuf. Syst.* **2018**, *1*, 97–114. [CrossRef]

3. Huang, X.; Zhao, L.; Chen, L. Numeric control machining technology research of millimeter wave slot antenna array. *Guid. Fuze* **2011**, *32*, 50–54.

4. Gilbin, A.; Fontaine, M.; Michel, G. Capability of tungsten carbide micro-mills to machine hardened tool steel. *Int. J. Precis. Eng. Manuf.* **2013**, *14*, 23–28. [CrossRef]

5. Lu, X.H.; Wang, F.R.; Wang, X.X.; Lu, Y.; Si, L. A surface roughness prediction model using response surface methodology in micro-milling Inconel 718. *Int. J. Mach. Mach. Mater.* **2017**, *19*, 230–245. [CrossRef]

6. Jing, X.; Lv, R.; Chen, Y.; Tian, Y.; Li, H. Modelling and experimental analysis of the effects of run out, minimum chip thickness and elastic recovery on the cutting force in micro-end-milling. *Int. J. Mech. Sci.* **2020**, *176*, 105540. [CrossRef]

7. Malekian, M.; Park, S.S.; Jun, M.B.G. Modeling of dynamic micro-milling cutting forces. *Int. J. Mach. Tool Manuf.* **2009**, *49*, 586–598. [CrossRef]

8. Rahman, M.A.; Rahman, M.; Kumar, A.S. Chip perforation and 'burnishing–like' finishing of Al alloy in precision machining. *Precis. Eng.* **2017**, *50*, 393–409. [CrossRef]

9. Sooraj, V.S.; Jose, M. An experimental investigation on the machining characteristics of microscale end milling. *Int. J. Adv. Manuf. Technol.* **2011**, *56*, 951–958. [CrossRef]

10. Ko, J.H.; Shaw, K.C.; Girsang, I.P.; Ravi, V.; Dhupia, J.S. Side-wall surface quality assessment for micro-end milling. *Int. Manuf. Sci. Eng. C* **2009**, *2*, 333–341.

11. Lu, X.H.; Jia, Z.Y.; Wang, H.; Si, L.; Wang, X. Surface roughness prediction model of micro-milling Inconel 718 with consideration of tool wear. *Int. J. Nanomanuf.* **2016**, *12*, 93–108. [CrossRef]

12. Shi, W.T.; Liu, Y.D.; Wang, X.B.; Jiang, F. Experiment and prediction model for surface roughness in micro-milling. *J. Agric. Mach.* **2010**, *41*, 211–215.

13. Burlacu, C.; Iordan, O. Mathematical modelling to predict the roughness average in micro milling process. *IOP C Ser. Mater. Sci. Eng.* **2016**, *145*, 072004. [CrossRef]

14. Bandapalli, C.; Sutaria, B.M.; Bhatt, D.V.; Singh, K.K. Experimental investigation and estimation of surface roughness using ANN, GMDH & MRA models in high speed micro end milling of titanium alloy (grade-5). *Mater. Today Proc.* **2017**, *4*, 1019–1028.

15. Bandapalli, C.; Sutaria, B.M.; Bhatt, D.V. Estimation of surface roughness on Ti-6Al-4V in high speed micro end milling by ANFIS model. *Indian J. Eng. Mater. Sci.* **2019**, *26*, 379–389.

16. Yazid, A.M.S. Modelling and Simulation of Surface Roughness Obtain from Micro Milling by Using Artificial Neural Network. Ph.D. Thesis, Universiti Tun Hussein Onn Malaysia, Parit Raja, Malaysia, 2014.

17. Allen, D.E.; Hooper, V. Generalized correlation measures of causality and forecasts of the VIX using non-linear models. *Sustainability* **2018**, *10*, 2695. [CrossRef]

18. Pusat, S.; Akkaya, A.V. Explicit equation derivation for predicting coal moisture content in convective drying process by GMDH-type neural network. *Int. J. Coal Prep. Util.* **2020**. [CrossRef]

19. Wang, X.X.; Lu, X.H.; Jia, Z.Y.; Jia, X.; Li, G.; Wu, W. Research on the prediction model of micro-milling surface roughness. *Int. J. Nanomanuf.* **2013**, *9*, 457–467. [CrossRef]